Prediction of Forest Attributes with Field Plots, Landsat, and a Sample of Lidar Strips: A Case Study on the Kenai Peninsula, Alaska

Jacob L. Strunk, Hailemariam Temesgen, Hans-Erik Andersen, and Petteri Packalen

Abstract

In this study we demonstrate that sample strips of lidar in combination with Landsat can be used to predict forest attributes more precisely than from Landsat alone. While lidar and Landsat can each be used alone in vegetation mapping, the cost of wall to wall lidar may exceed users' financial resources, and Landsat may not support the desired level of prediction precision. We compare fitted linear models and k nearest neighbors (kNN) methods to link field measurements, lidar, and Landsat. We also compare 900 m² and 8,100 m² resolutions to link lidar to Landsat. An approach with lidar and Landsat together reduced estimates of residual variability for biomass by up to 36 percent relative to using Landsat alone. Linear models generally performed better than kNN approaches, and when linking lidar to Landsat, using 8,100 m² resolution performed better than 900 m².

Introduction

Studies which demonstrate ways to use lidar in forest inventory, mapping, and monitoring are now fairly common. Investigators have modeled and estimated forest attributes (Tonolli *et al.*, 2011; Strunk *et al.*, 2012a) classified forest types (Pascual *et al.*, 2008) species (Kim *et al.*, 2009a; Zhang and Qiu, 2012), and condition (Kim *et al.*, 2009b), delineated stand boundaries(Sullivan *et al.*, 2009), and segmented upper canopy tree crowns (Hyyppa *et al.*, 2001). These and most other studies demonstrate approaches which rely on complete lidar coverage for their area of interest (AOI). However, the acquisition of lidar for an entire AOI is not always justifiable due to high costs, especially for large AOIs.

Recently, interest has increased in approaches to estimate forest attributes from a sample of lidar strips (or swaths) (Gregoire *et al.*, 2011; Ståhl *et al.*, 2011; Andersen *et al.*, 2011a). Unfortunately, while a sample of lidar strips is less expensive than complete lidar coverage, a sample of lidar strips is not directly suited to mapping. To map between the strips requires an additional source of auxiliary information. One option is to fill in the gaps between lidar strips using lower cost reflectance information collected with a passive remote sensing technology such as Landsat or aerial photography.

Jacob L. Strunk and Hailemariam Temesgen are with the Department of Forest Engineering, Resources and Management, Oregon State University, Corvallis, OR, 97331 (Jacob.Strunk@oregonstate.edu).

Hans-Erik Andersen is with the USDA Forest Service PNW Research Station, Seattle, WA.

Petteri Packalen is with the Faculty of Science and Forestry, University of Eastern Finland, Joensuu, Finland.

The use of lidar with alternate sources of remote sensing has also been demonstrated in the literature; although most efforts used combined lidar and spectral information when both were available for the same areas (Packalén and Maltamo, 2006; Hudak *et al.*, 2006; Popescu *et al.*, 2004). Fit statistics for models developed in these studies did not appear to appreciably improve when spectral information is used in addition to lidar. Spectral information can provide improvements in species differentiation over lidar alone (e.g., Ørka *et al.*, 2012). There are also examples of studies for which lidar was only available for a subset of the AOI, while spectral information was available over a broader area. Wulder *et al.* (2007) used Landsat Enhanced Thematic Mapper (ETM+) data and successive profiling lidar measurement to study change in vertical height over a period of time. Landsat data were used to segment the region, and then lidar was used to assign height data for the segments in successive lidar acquisitions. The authors found this approach to be more effective for detecting change than simply differencing the strips. A similar approach by Andersen *et al.* (2011b) used Landsat and polarimetric SAR to classify the landscape with a nearest neighbor approach to classify the landscape. Scanning lidar data were then used to estimate average biomass for the classes. The approach was aimed at estimation (e.g., of the population mean or total) rather than prediction (e.g., for mapping). A similar approach by Chen and Hay (2011) for a small test area compared multiple regression and support vector machines to relate characteristics of image segments to lidar data; although unlike in Andersen *et al.* (2011b), the image segments were individual tree crowns.

In a study by Hudak *et al.* (2002) simulations were used to look at estimation of canopy height from Landsat ETM+ and samples of lidar data for different numbers and configurations of lidar samples. The authors compared a variety of approaches including geo-statistical models and were successful in improving the precision of predictions for areas not covered with lidar. However, with 2000 m being the greatest distance between lidar measurements, it is not clear how well these approaches would perform for lower lidar sampling intensities (e.g., the sampling intensities used by Andersen (2009), Andersen *et al.* (2011a), Gregoire *et al.* (2011), and Ståhl *et al.* (2011).

We consider the modeling approach to be of great importance in evaluating a prediction strategy, both in terms of performance (precision) and utility. Two common approaches to

Photogrammetric Engineering & Remote Sensing
Vol. 80, No. 2, February 2014, pp. 000–000.
0099-1112/14/8002–000

doi: 10.14358/PERS.80.2.000

model forest attributes from remote sensing are ordinary least squares (OLS) for linear models (Means *et al.*, 2000; Strunk *et al.*, 2012b) and kNN imputation (Maltamo *et al.*, 2006; Packalén and Maltamo, 2007). Linear models can precisely predict (low RMSE relative to variability in the response) a variety of continuous forest attributes including basal area (Jensen *et al.*, 2006; Means *et al.*, 2000), volume (Næsset, 1997; Lim *et al.*, 2003), and biomass (Drake *et al.*, 2003; Hall *et al.*, 2005). Nearest neighbor approaches also perform well (low RMSE) in the prediction of these variables, and we consider them to be much more user friendly and operationally useful because they can be used to predict a variety of forest attributes, including diameter distributions by species (Packalén and Maltamo, 2008), i.e., required information for most operational forest inventories.

The objective of this study was to evaluate whether using lidar in addition to Landsat for prediction of forest attributes (biomass, basal area, and number of trees) could improve the precision of forest attribute predictions from Landsat and by how much. To investigate our research question, we compared multiple strategies to link Landsat to field measurements and lidar. We compared both linear models fitted with ordinary least squares (OLS) and k nearest neighbors (kNN) as approaches to link Landsat to field measurements and lidar; kNN was examined using multiple distance metrics. We also examined two configurations to link lidar to Landsat including (a) using lidar-based predictions of forest attributes to train Landsat models, and (b) relating lidar directly to Landsat and using predicted lidar variables as explanatory variables in predictions of forest attributes. Finally, to evaluate the effect of resolution, lidar measurements were linked to Landsat at both 900 m² and at 8,100 m². The multiple approaches were evaluated according to their estimated residual variability. To enable the evaluations we developed an estimator of residual variance for predictions from a strategy with more than one model.

Methods

Study Site

Our study was conducted for the boreal forests located in the western lowlands, an area of the 8,200 km² on the Kenai Peninsula in Alaska (Figure 1). The extent of our study area was restricted to the portion of the western lowlands that falls within a single Landsat image, approximately 7,400 km². Prevalent forest types for this area include black spruce (*Picea mariana*, 23 percent of measured trees) in wet lower parts of drainages, and mixed paper birch (*Betula papyrifera*, 19 percent of measured trees), white spruce (*Picea glauca*, 47 percent of measured trees), and quaking aspen (*Populus tremuloides*, 10 percent of measured trees) in well drained areas. The study area ranged in height above sea level from 0 to 700 m with the majority (65 percent) of the AOI falling below 150 m. Aside from a narrow band on the northern border of the study area, areas outside of our study area on the peninsula are dominated by the mountains.

Forest Measurement Data

Data for this study were collected as part of the US Forest Service (USFS) Forest Inventory and Analysis (FIA) annual inventory program. The FIA field plots area arranged in a ten-panel design and that each field plot consisted of four circular 168 m² subplots arranged in a fixed manner with respect to distance and orientation from plot center (Bechtold and Patterson, 2005). Unlike other parts of the country, the systematic sample of FIA plots on the Kenai Peninsula has a single randomization. The field measurements used in this study were collected between 2005 and 2009. Measurements were obtained for trees greater than 12.7 cm in diameter. For our analysis, we used a subset of 32 field plots including 89 subplots (Table 1) from the systematic grid of field plots covering our AOI. A survey-grade GPS receiver was used to obtain precise (less than 0.5 m horizontal RMSE) coordinates for this subset of FIA plots (Andersen *et al.*, 2009). Tree height, diameter, species, condition class (live or dead), and above ground live biomass from the FIA database were used. Response variables included biomass per hectare (bio), basal area per hectare (ba), and stems per hectare (stems). Response values were calculated from individual tree records and then aggregated for plots.

TABLE 1. SUMMARY OF RESPONSE DATA FOR 80 SUBPLOTS USED IN ANALYSES

	Minimum	Maximum	Mean	SD
Total biomass (bio kg/ha)	0	179,002	35,421	45,572
Basal area (ba m²/ha)	0	32.9	8.3	9.1
stems /ha	0	1,130	227	242
Total height (m)	1.5	25.3	12.4	4.7
DBH (cm)	12.9	56.9	20.8	7.1

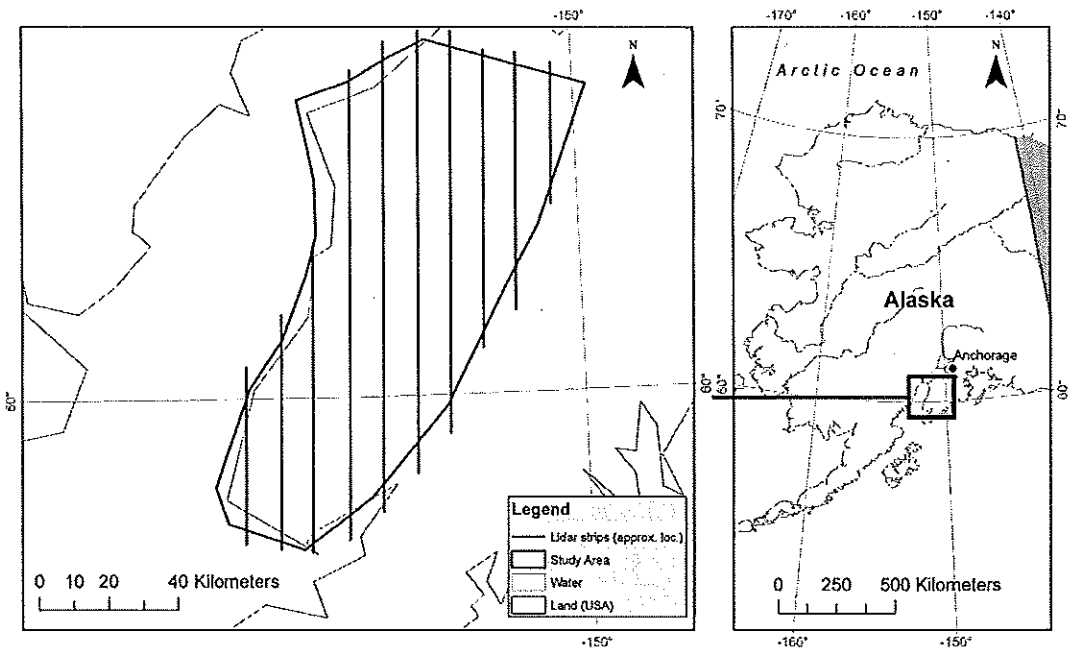

Figure 1. Location of study area on the Kenai Peninsula, Alaska

Lidar

Airborne discrete-return scanning lidar data (lidar) were collected in leaf-off condition for the Kenai Peninsula in the spring of 2009. Lidar data were collected in a systematic sample of strips over the locations of a subset of the grid of FIA field plots on the peninsula. The average flying height was 1,150 m above ground, the maximum half scan angle was 7.5 degrees, the average flying speed was 66 meters/sec, and the pulse repetition frequency was approximately 71 kHz. The flight configuration yielded a nominal pulse density of 4 pulses / m^2.

Lidar data consists of a series of records corresponding to locations ("returns") where pulses within laser scan lines intersected the ground or objects above the ground. We are specifically interested in the vertical distribution of lidar returns within an area (e.g., a plot) which provide information regarding the vertical arrangement of bole wood, branches, and foliage. Lidar data were summarized using statistics computed on first return lidar heights (these lidar statistics are henceforth referred to as "lidar metrics"). Lidar heights are lidar point elevations minus ground elevations for the same horizontal coordinates. The point data were processed to extract lidar metrics for circles centered on field plot locations with 13 m, 30 m, and 90 m radii. Lidar metrics considered in our analyses included height percentiles (e.g., ht_{95} is the 95th percentile lidar height computed from all of the first-return lidar heights in the plot greater than 1 m) and cover ratios (e.g., $cover_1$ is the proportion of first returns above 1 m). Lidar data were processed, including identification of ground returns and interpolation of a digital terrain model, using the freely-available FUSION software (McGaughey, 2012). The extensive list of lidar metrics provide by FUSION can be found in the FUSION manual.

Landsat

Our analyses made use of the historical archive of Landsat TM and Landsat ETM+ imagery available from the GLOVIS website (*http://glovis.usgs.gov/*). We selected late spring through early fall Landsat images from the years 1984 to 2009. We used only images that had cloud-free areas intersecting our AOI. Landsat ETM+ images were used from both scan line corrector (SLC) on (1999 to 2003), and SLC off (after May 2003) periods.

Landsat data were used in this study by taking advantage of the trajectories of individual pixel values over time. Ideally, the value recorded for a Landsat pixel is related to static vegetation properties (i.e., properties that are constant over a short period, such as a year) for the corresponding location on the ground. However, the value recorded for a given pixel is influenced by a wide range of factors including phenology, atmospheric conditions, solar incidence angle, sensor properties, and others. For our purposes, these factors were all considered noise. If we assume these sources of noise are random, then for a pixel representing a static ground condition, we can average values from multiple years to obtain a more representative, less noisy pixel value. However, ground conditions are rarely static and the average pixel values for a given location over time may incorporate temporal noise. The LandTrendr process (Kennedy *et al.*, 2010) is an approach that empirically accounts for change over time in the predictor variables using piecewise linear regression. This removes time as a source of variation and makes it possible to average across pixels in time. We note, however, that modeling changes in temporal values in this exercise is just a means to an end; our objective is to have a source of explanatory information with a reduced level of noise. We are not attempting to predict changes in vegetation over time; we are attempting to eliminate temporal changes as a source of noise in our explanatory variables.

For most parametric modeling strategies, predictions near the bounds of the fitting data tend to be less stable than predictions near the center. The same is true of temporal trajectories with Landsat pixels. In our case 1984 and 2009 were the bounds of our trajectories. To mitigate this variation we used fitted values for 2007 as predictors for our analysis. We fitted pixel-based time-series models for Landsat bands 1 to 5, and 7, as well as the derivative vegetation indices normalized burn ratio (NBR), and normalized difference vegetation index (NDVI). Pixel values were interpolated to sample locations from surrounding cells by taking the averages of pixels with center points within 30 m and 90 m radii.

A beneficial side-effect of this approach is that we can predict cloud-free values for a pixel for any point in the time series. This an important benefit given the difficulty in finding cloud-free images in Alaska, the irregularities in ETM+ data after May 2003 caused by the failure of an important sensor component, the scan line corrector, for Landsat-7, and the failure of the Landsat-5 sensor (November 2011).

Model Development

In this study we refer to model development as the process of linking response and predictor variables via an empirical relationship to enable predictions of response values. In this study we make use of both kNN imputation and linear models fitted with OLS to predict response values from predictor variables. kNN imputation (where impute means to substitute for a missing value) is a well-known non-parametric approach to link response and predictor variables. In a kNN strategy, response values from one to many (k) observations with measured response values (reference observations) are imputed to observations for which only the predictor variables are measured (target observations). Selection of a specific group of k observations from the reference set, or donors, to impute response values to a target observation is based upon the distance between the observations in predictor space. For all practical purposes the words "impute" and "predict" can be treated as synonymous, and henceforth we use the word "predict" in place of "impute."

In preliminary investigations for this study, RMSEs for kNN prediction strategies were largely insensitive to the choice of k in the range of three to fifteen neighbors. We arbitrarily set k to five neighbors and predicted the value of the response value as the inverse distance weighted average of the five nearest neighbors. The choice of distance metric plays an important role in kNN and has a significant role in performance. In this study, we examined four measures of distance for nearest neighbor approaches in this study. The first distance approach was Euclidean distance based on normalized predictors (kNN-EU). The second was weighted Euclidean distance with weights assigned according to the magnitudes of the coefficients when canonical correlation was used to relate normalized response and predictor variables (kNN-MSN). The third approach was based on distances calculated from a random forest proximity matrix (kNN-RF). The fourth approach was Mahalanobis distance (kNN-MH).

Linking Field Plots to Landsat

Direct and indirect approaches were used to link field measurements to remote sensing data. In the direct approach, Landsat was linked to field measurements with a model:

$$y = \hat{f}_1(\mathbf{x}) + \hat{\varepsilon}_1 \tag{1}$$

where x is the matrix of Landsat variables for sample, y is the response variable for sample, $\hat{f}_1(.)$ is a fitted model relating x and y, for example, and $\hat{\varepsilon}_1$ is a vector of random noise.

The model $\hat{f}_1$ was then used with wall-to-wall Landsat to predict the response variable for the landscape:

$$\hat{Y} = \hat{f}_1(\mathbf{X}) \tag{2}$$

where X is the matrix of Landsat variables for landscape, and $\hat{Y}$ is the predictions from $\hat{f}_1$ for landscape.

Similarly we directly related the response to lidar for the field sample:

$$Y = \hat{f}_2(z) + \hat{\varepsilon}_2 \quad (3)$$

where z is the matrix of lidar variables for sample, Y is the response variable for sample, and $\hat{\varepsilon}_2$ is the vector of random noise.

However, unlike with Landsat, we only had lidar variables for a subset of the landscape (the lidar strips) and thus could only directly predict our response for a subset of the landscape:

$$\hat{Y}^* = \hat{f}_2(Z^*) \quad (4)$$

where Z^* is the matrix of Landsat variables for strips, and $\hat{Y}^*$ is the predictions from $\hat{f}_2$ for strips.

Our first of two indirect modeling strategies (I.A) to circumvent this limitation was to predict the values of lidar metrics for the entire landscape from Landsat. To do this we first related our Landsat variables to our lidar variables:

$$Z^* = \hat{f}_3(X^*) + \hat{\varepsilon}_3 \quad (5)$$

where X^* is the matrix of Landsat variables for strips, and $\hat{\varepsilon}_3$ is the matrix of residuals for lidar variables.

We then used $\hat{f}_3$ to predict our lidar variables for the landscape:

$$\hat{Z} = \hat{f}_3(X) \quad (6)$$

where $\hat{Z}$ is the matrix of predicted lidar variables for landscape.

With the predicted matrix Z of lidar variables we used $\hat{f}_2$ to predict our response for the landscape:

$$\hat{Y} = \hat{f}_2(\hat{Z}). \quad (7)$$

In the second indirect modeling strategy (I.B), predicted forest attributes were modeled with Landsat:

$$\hat{Y}^* = \hat{f}_4(X^*) + \hat{\varepsilon}_4 \quad (8)$$

where $\hat{f}_4$ is the model relating $\hat{Y}^*$ and X^*, and $\hat{\varepsilon}_4$ is the vector of residuals.

In this case the Landsat and the predicted forest attributes are of matched resolutions, which differ from the resolution of the field measurements. After fitting $\hat{f}_4$ we then predicted our response variable for the landscape using Landsat:

$$\hat{Y} = \hat{f}_4(X). \quad (9)$$

The resolution used to relate lidar to Landsat was different from the resolution used to relate lidar to the field plots. When we related lidar to our forest attributes from the field plot, we used the subplot area which was 168 m². When we related lidar to Landsat, we could comfortably use any resolution coarser than 900 m², and in this study we examined 900 m² and 8100 m².

Variance Estimation

Theory

Part of our modeling effort (indirect models I.A and I.B) included two steps. Here, we use basic statistical principles to develop a variance estimator for this case. We began by examining generic model f_1 used to relate a response variable to explanatory variables:

$$Y = f_1(Z) + \varepsilon_1 \quad (10)$$

where Z is the matrix of predictor values, Y is the response variable, and ε_1 is a vector of random noise.

Predictions from f_1 can be obtained from explanatory information:

$$\hat{Y} = f_1(Z^*) \quad (11)$$
$$= \text{predicted response value for some values } Z^* \in Z$$
$$= \hat{Y} - \varepsilon_1.$$

A second model f_2 described the relationship between our predicted response and an alternate set of predictor variables:

$$\hat{Y} = f_2(X) + \varepsilon_2 \quad (12)$$

where X is the matrix of alternate predictor variables, and ε_2 is a second vector of random noise.

We can see that because f_2 was fitted to predictions of the response, we now have two sources of error:

$$\hat{Y} = Y - \varepsilon = f_2(X) + \varepsilon_2 \quad (13)$$
$$Y = f_2(X) + \varepsilon_1 + \varepsilon_2.$$

The variance of Y given X can then be expressed by recognizing that it is the variance of a sum of error terms:

$$V[Y|Z] = V[\varepsilon_1 + \varepsilon_2] = V[\varepsilon_1] + V[\varepsilon_2] + 2 \times cov(\varepsilon_1, \varepsilon_2) \quad (14)$$

where $V[.]$ is the variance of, and $cov(\varepsilon_1, \varepsilon_2)$ is the covariance of ε_1 and ε_2.

A variance estimator can be developed from consistent estimators for the various components:

$$V[Y|Z] \approx v[\hat{\varepsilon}_1] + v[\hat{\varepsilon}_2] + 2 \times cov(\varepsilon_1, \varepsilon_2) \quad (15)$$

where $v[\hat{\varepsilon}_1]$ and $v[\hat{\varepsilon}_2]$ are estimates of $V[\varepsilon_1]$ and $V[\varepsilon_2]$, $cov(\varepsilon_1, \varepsilon_2)$ is the estimated covariance of ε_1 and ε_2, and $\hat{\varepsilon}_1$ and $\hat{\varepsilon}_2$ are residuals from fitted models $\hat{f}_1$ and $\hat{f}_2$.

A modification to the described variance estimation strategy was necessary for our first indirect strategy, Equations 5 through 7, because in Equation 5 we do not have residuals for the response variable due to the fact that we were modeling lidar metrics with Landsat. For this step the residuals $\hat{\varepsilon}_2$ in Equation 15 are estimated as the difference between predictions of the response with $\hat{f}_2$ from the original lidar values for the lidar strips and from the fitted lidar values:

$$\hat{\varepsilon}_2 = \hat{f}_2(Z^*) - \hat{f}_2(\hat{Z}^*). \quad (16)$$

Estimators

The components of our variance estimators ($v[\hat{\varepsilon}_1]$, $v[\hat{\varepsilon}_2]$ and $cov(\hat{\varepsilon}_1, \hat{\varepsilon}_2)$) were estimated using a leave-k cross-validation strategy (not to be confused with k-folds cross validation) for field plots. Residuals were estimated by omitting entire plots (consisting of multiple subplots) at one time. Residual variance was estimated as:

$$\hat{\sigma}^2_{\hat{\varepsilon}} = \frac{1}{kN} \sum_{o=1}^{kN} (\hat{Y}_o - Y_o)^2 \quad (17)$$

where $\hat{\sigma}^2_{\hat{\varepsilon}}$ is the plot observation omitted from model fitting procedure, k is the number of observations omitted in an iteration, N is the number of simulations, $\hat{Y}_o$ is the prediction for omitted observation (plot), and Y_o is the observed response for omitted observation (plot).

We opted for a leave-k-out (k >1) strategy because we found that the estimator was more likely to converge to the apparent error rate for a small sample than a leave-1-out strategy. A leave-k strategy will be increasingly conservatively

biased for increasing values of k, but the bias will be small for small values of k, and will provide an estimator with considerably reduced variance. This was evident when we tracked our standard error values for the leave-k-out estimator with k = 3. As can be seen in Figure 2, the estimator was highly variable for fewer than 200 simulations. Efron and Tibshirani (1993, pp. 148–149) provide some discussion of failure from the related jackknife estimator. For a sample with more than 200 observations, we could reasonably have used the leave-1-out estimator, but since our sample only had 32 plots, the sampling distribution of the estimator would have been highly variable.

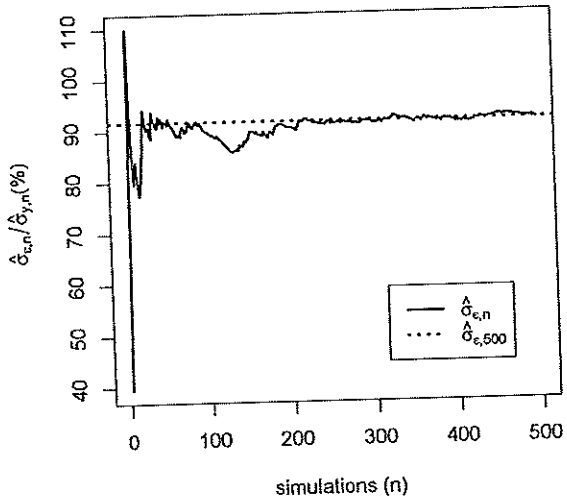

Figure 2. Visual diagnostic of convergence relative to number of simulations for a leave-3-out estimator of residual standard deviation.

Direct models relating field plot measurements to remote sensing data were fitted using the 80 subplots with field measurements, lidar, and Landsat. A slightly larger proportion of the landscape was used to relate lidar to Landsat. Using a larger number of observations on average improves the performance of these models. While the number of values with both lidar and Landsat was quite large, to expedite simulations we restricted our analyses to a subset of 1,500 locations on the Kenai Peninsula with both lidar and Landsat. Calculations for each configuration required extensive processing time, particularly for approaches involving kNN. We used 1,500 points because preliminary tests showed that more than 1,500 observations did not appreciably affect estimates of residual variability. The 1,500 points were obtained by distributing a systematic grid within the lidar strips. The 1,500 random points were in addition to the 80 subplots that had field measurements, lidar, and Landsat. Models relating lidar and Landsat were developed from all 1,500 random points and 80 subplots, but the residual variability was estimated using residuals for the 80 subplots; the models were fitted to individual subplots, but residual variability was estimated by simultaneously omitting all subplots corresponding to a plot.

Results

Modeling strategies were evaluated according to their RMSE values. The strategies were designated by the sequential order of models included in the strategy. For example for an indirect strategy kNN-MH OLS indicates a modeling strategy in which kNN-MH was used to link lidar to field plots and OLS was used to link lidar to Landsat.

RMSE values for models directly linking lidar and field plots are provided in Table 2. The results are much better than models linking field plots to Landsat directly, shown in Table 3, which was the expected result. However, the RMSE values for lidar serve only as a benchmark for comparison; a direct lidar to field plot modeling approach is not a viable mapping strategy when lidar is collected as a sample of strips. For both lidar and Landsat, OLS models performed better on average than alternate model types. kNN-RF performed only slightly worse in most cases, and both kNN-RF and kNN-EU performed better than OLS for numbers of stems/ha for lidar.

Table 2. RMSE Values (And Percent Relative To The Between Plot Variability) For Direct Prediction Strategy With Lidar For Approaches Used To Link Lidar To Field Plots

	$\hat{\sigma}_{\varepsilon,2P}$ ($\hat{\sigma}_{\varepsilon,2P}/\hat{\sigma}_{Y,SRS}\times100\%$)					
Models	**bio kg/ha (%)**		**ba m²/ha (%)**		**stems/ha (%)**	
OLS	21061	(44%)	5.0	(52%)	193	(77%)
kNN-MSN	23786	(50%)	5.5	(58%)	213	(85%)
kNN-RF	22395	(47%)	4.9	(52%)	184	(73%)
kNN-EU	23880	(50%)	5.1	(54%)	177	(70%)
kNN-MH	28734	(60%)	6.2	(66%)	219	(87%)

Table 3. RMSE Values (And Percent Relative To The Between Plot Variability) For Direct Prediction Strategy With Landsat For Approaches Used To Link Landsat To Field Plots

	$\hat{\sigma}_{\varepsilon,2P}$ ($\hat{\sigma}_{\varepsilon,2P}/\hat{\sigma}_{Y,SRS}\times100\%$)					
Models	**bio kg/ha (%)**		**ba m²/ha (%)**		**stems/ha (%)**	
OLS	43115	(92%)	8.4	(90%)	228	(93%)
kNN-MSN	48344	(104%)	9.3	(100%)	243	(99%)
kNN-RF	46053	(99%)	8.8	(95%)	233	(94%)
kNN-EU	48862	(105%)	9.4	(101%)	237	(96%)
kNN-MH	48663	(104%)	9.2	(100%)	237	(96%

The performance of the two indirect modeling strategies were highly dependent upon whether 900 m² or 8,100 m² resolution was used to link lidar and Landsat. For the 900 m² resolution (Tables 4 and 5) the performance for the first indirect strategy (I.A) was superior to the second (I.B) in terms of RMSE for biomass and volume for nearly every modeling configuration. This was especially true for biomass, although the poorest performing I.A approaches were exceeded by the best I.B approaches. Number of stems/ha at 900 m² resolution was the only example in which strategy I.B appears to be generally superior. Both I.A and I.B strategies saw improvement from using 8,100 m² resolution data in linking lidar to Landsat, but the improvement was minimal for strategy I.B. For strategy I.A, improvements were substantial for all three of the response variables for several combinations of models.

Among the RMSE values reported for the various strategies in Tables 3 through 6, some of the modeling approaches consistently performed better than others. kNN-MH OLS, for example, was competitive in nearly every case. The OLS OLS approach also generally performed well, and for I.A with 900 m² resolution performed the best of any of the strategies examined. Excluding OLS OLS, it appears that approaches using kNN model followed by OLS performed the best for biomass (See Table 7). There was no clear difference between these two groups for volume, and OLS followed by a kNN approach worked best for number of stems/ha.

Table 4. RMSE Values (And Percent Relative To The Between Plot Variability) For Indirect Modeling Strategy I.A For The Approaches Used To Link Field Plots To Lidar And Landsat When Lidar And Landsat Were Linked At 900 M² Resolution

Models	$\hat{\sigma}_{\varepsilon,3P}$ ($\hat{\sigma}_{\varepsilon,3P}$ / $\hat{\sigma}_{Y,SRS}$ ×100%)		
	bio kg/ha (%)	ba m²/ha (%)	stems/ha (%)
OLS OLS	38288 (80%)	7.8 (82%)	229 (91%)
OLS kNN-MSN	43630 (91%)	8.6 (91%)	241 (96%)
OLS kNN-RF	41474 (86%)	8.3 (88%)	238 (94%)
OLS kNN-EU	42183 (88%)	8.2 (87%)	234 (93%)
OLS kNN-MH	45084 (94%)	8.9 (94%)	249 (99%)
kNN-MSN OLS	39587 (82%)	8.8 (93%)	302 (120%)
kNN-RF OLS	37357 (78%)	8.0 (85%)	268 (106%)
kNN-EU OLS	33652 (70%)	7.6 (81%)	258 (103%)
kNN-MH OLS	33161 (69%)	7.8 (83%)	295 (117%)

Table 5. RMSE Values (And Percent Relative To The Between Plot Variability) For Indirect Modeling Strategy I.B For The Approaches Used To Link Field Plots To Lidar And Landsat When Lidar And Landsat Were Linked At 900 M² Resolution

Models	$\hat{\sigma}_{\varepsilon,3P}$ ($\hat{\sigma}_{\varepsilon,3P}$ / $\hat{\sigma}_{Y,SRS}$ ×100%)		
	bio kg/ha (%)	ba m²/ha (%)	stems/ha (%)
OLS OLS	43159 (90%)	8.3 (88%)	222 (88%)
OLS kNN-MSN	43742 (91%)	8.7 (92%)	222 (88%)
OLS kNN-RF	46336 (97%)	9.2 (98%)	227 (90%)
OLS kNN-EU	46112 (96%)	9.2 (97%)	226 (90%)
OLS kNN-MH	45582 (95%)	9.1 (96%)	221 (88%)
kNN-MSN OLS	45264 (94%)	9.3 (98%)	259 (103%)
kNN-RF OLS	44800 (93%)	8.6 (91%)	216 (86%)
kNN-EU OLS	44053 (92%)	8.7 (92%)	221 (88%)
kNN-MH OLS	39764 (83%)	8.3 (87%)	249 (99%)

Table 6. RMSE Values (And Percent Relative To The Between Plot Variability) For Indirect Modeling Strategy I.B When Lidar And Landsat Were Linked At 8,100 M² Resolution

Models	$\hat{\sigma}_{\varepsilon,3P}$ ($\hat{\sigma}_{\varepsilon,3P}$ / $\hat{\sigma}_{Y,SRS}$ ×100%)		
	bio kg/ha (%)	ba m2/ha (%)	stems /ha (%)
OLS OLS	28538 (59%)	6.1 (64%)	203 (81%)
OLS kNN-MSN	35550 (74%)	7.3 (77%)	213 (85%)
OLS kNN-RF	36543 (76%)	7.5 (79%)	217 (86%)
OLS kNN-EU	37144 (77%)	7.8 (82%)	222 (88%)
OLS kNN-MH	37347 (78%)	7.8 (82%)	215 (85%)
kNN-MSN OLS	30960 (65%)	7.5 (79%)	258 (103%)
kNN-RF OLS	31044 (65%)	7.1 (75%)	243 (97%)
kNN-EU OLS	29562 (62%)	6.8 (72%)	244 (97%)
kNN-MH OLS	29358 (61%)	6.3 (67%)	238 (95%)

Table 7. RMSE Values (And Percent Relative To The Between Plot Variability) For Indirect Modeling Strategy I.B For The Approaches Used To Link Field Plots To Lidar And Landsat When Lidar And Landsat Were Linked At 8,100 M² Resolution

Models	$\hat{\sigma}_{\varepsilon,3P}$ ($\hat{\sigma}_{\varepsilon,3P}$ / $\hat{\sigma}_{Y,SRS}$ ×100%)		
	bio kg/ha (%)	ba m²/ha (%)	stems0/ha (%)
OLS OLS	35017 (73%)	7.7 (81%)	218 (87%)
OLS kNN-MSN	39583 (82%)	8.3 (88%)	224 (89%)
OLS kNN-RF	42257 (88%)	8.8 (93%)	224 (89%)
OLS kNN-EU	42409 (88%)	8.8 (93%)	224 (89%)
OLS kNN-MH	41174 (86%)	8.6 (91%)	230 (91%)
kNN-MSN OLS	38191 (80%)	8.6 (91%)	251 (100%)
kNN-RF OLS	37894 (79%)	7.9 (84%)	231 (92%)
kNN-EU OLS	35129 (73%)	7.5 (79%)	209 (83%)
kNN-MH OLS	36697 (76%)	8.2 (87%)	264 (105%)

Discussion

Multi-level Modeling Strategies

We examined both direct and indirect strategies to link Landsat to field measured attributes. The direct strategy with plot and Landsat data had the poorest performance; our later analyses of 900 m² and 8,100 m² resolutions suggest that plot size played a role. Our findings also suggest that a direct Landsat approach would be more successful with a larger number of plots. Conceivably, if the area covered by four subplots per FIA plot were consolidated into a single larger plot, the performance of Landsat models would be improved for the forest attributes examined herein. However, such a plot design would provide less information about variables not effectively modeled with lidar, and in many cases large Landsat-optimized plot designs (e.g., 8,100 m² in area) would either not be affordable or compatible with existing designs. Lidar provides an opportunity to help bridge the gap between field plots and Landsat in such cases; FIA plots are an example of a design that will continue to benefit from the use of lidar to bridge the gap. This was especially true for our study area where a lidar strip can be substantially less expensive than a field plot. If performance can be improved for variables associated with forest structure by leveraging lidar, then it may be possible to devote more energy to measuring variables which are more difficult to predict with remote sensing.

Our analyses also showed that the first indirect modeling strategy (I.A) appeared to perform better, on average, than the second (I.B), but that there was wide variation in performance depending on which type of model was used to link the various layers of data. Prediction performance for indirect strategies also improved when we used larger areas to relate lidar to Landsat; although the degree of improvement also varied considerably depending upon the types of models used. The best overall performance was seen with modeling strategy I.A for 8,100 m² resolution in which linear models fit with OLS were used to link field plots and remote sensing. The performance of this approach may further improve in instances where coarser resolutions are used to relate lidar and Landsat because the proportion of overlapping areas between lidar and Landsat would increase, reducing the impacts of edge effects, registration errors, and noise.

Limitations

There were a variety of limitations in our study with respect to the training dataset which restricted our ability to explore different modeling scenarios. As a result, the findings we

present here are certainly not the last word on the issues explored in this study, even for our study area. For example, many of our field measurements were not collected simultaneously with the lidar data. Field measurements spanned a five year period, while lidar data were collected in 2009, the fifth year of field data collection. Furthermore, the number of training observations was small, and the size of subplots was quite small. As a result, we cannot speculate on the performance of our approach under ideal conditions. However, given that we were able to explain more variability with indirect approaches than with a direct approach with Landsat; our results still indicate that using lidar to scale up the plot data to the resolution of the Landsat data is a promising approach. This is especially the case if a lidar strip sampling approach is already in place or under consideration for estimation purposes.

A second limitation which has been suggested is that we do not attempt to separate the effect of within-plot variability from improved model performance when we compare models developed at different resolutions. In alternate cases this could be problematic because variability between plots will decline as variability within plots increases. For single circular plots, as the area of the plots increases the variability between plots will decrease. However, an advantage of the FIA plot design is that while the total area of the subplots is approximately 670 m², the subplots sample spatial variability for a much larger 6,000 m² area. Since our validation was performed using FIA plots consisting of multiple subplots, the resolutions considered are of limited concern.

Multi-temporal Landsat

We were able to make use of the freely-available Landsat archive to generate atmospherically corrected, cloud-free, and temporally normalized Landsat values. The temporal signal enabled us to identify and remove variability in the sensed values for a particular pixel location for a particular spectral band which are not associated with changes in the associated vegetative structure. However, this could be considered an under-utilization of this resource, and we envision greater success in the prediction of forest attributes if the trend information, such as intercept for the trend, or the slope or information about large perturbations are taken into consideration as described in Meigs *et al.* (2011), Kennedy *et al.* (2007), Powell *et al.* (2010), and Pflugmacher (2011). At this time we have insufficient information to determine whether LandTrendr data for image processing improved the performance for cloud-free pixels, but since there are no recent Landsat images available for the Kenai Peninsula that are 100 percent cloud free, we can say that we were able to develop predictions for all areas on the peninsula which would not be possible with a single image. In the future we plan to quantify any gains made by using this approach for cloud-free pixels, as well as the potential gains made using a more sophisticated interpretation of Landsat time-series information for individual pixels.

Conclusions

Using lidar strips as a sample can be an efficient strategy to leverage the forest structure information measured by lidar, while collecting the data for a reduced cost relative to a complete area collection. This strategy is chiefly aimed at point estimation (e.g., total biomass for an area), but we demonstrate in this study that lidar strips can also be useful in training coarser resolution Landsat data for prediction of forest attributes including biomass, volume, and trees per hectare. We explored a number of approaches and found that linking plot data to lidar and lidar to Landsat in separate steps before predicting forest attributes with Landsat improved the precision of predictions (lower RMSE). We also found that using 8,100 m² resolution to link lidar to Landsat performed better than with 900 m² resolution. Moving to an even larger area for linking lidar to Landsat may also prove beneficial.

While we performed our analyses only for a sample of locations on the peninsula in our exploratory investigations, the use of Landsat-derived layers enables predictions across the entire AOI.

Acknowledgments

We would like to express our appreciation to Robert E. Kennedy and Justin Baaten for their guidance and assistance with LandTrendr. We would also like to thank Lisa Madsen for her comments and suggestions on an initial draft. Finally, we wish to recognize the excellent feedback from two anonymous reviewers.

Funding and data for this study were graciously provided by USFS-PNW research station.

References

Andersen, H.-E., 2009. Using airborne light detection and ranging (LIDAR) to characterize forest stand condition on the Kenai Peninsula of Alaska, *Western Journal of Applied Forestry*, 24(2):95–102.

Andersen, H.-E., T. Clarkin, K. Winterberger, and J.L. Strunk, 2009. An accuracy assessment of positions obtained using survey-and recreational-grade global positioning system receivers across a range of forest conditions within the Tanana Valley of interior Alaska, *Western Journal of Applied Forestry*, 24(3):128–136.

Andersen, H.-E., J. Strunk, and H. Temesgen, 2011a. Using airborne light detection and ranging as a sampling tool for estimating forest biomass resources in the upper Tanana Valley of interior Alaska, *Western Journal of Applied Forestry*, 26(4):157–164.

Andersen, H.-E., J. Strunk, H. Temesgen, D. Atwood, and K. Winterberger, 2011b. Using multilevel remote sensing and ground data to estimate forest biomass resources in remote regions: A case study in the boreal forests of interior Alaska, *Canadian Journal of Remote Sensing*, 37(6):596–611.

Bechtold, W.A., and P.L. Patterson (editors), 2005. *The Enhanced Forest Inventory and Analysis Program: National Sampling Design and Estimation Procedures*, US Department of Agriculture Forest Service, Southern Research Station, Asheville, North Carolina. 85 p.

Chen, G., and G.J. Hay, 2011. A support vector regression approach to estimate forest biophysical parameters at the object level using airborne lidar transects and QuickBird data, *Photogrammetric Engineering & Remote Sensing*, 77(7):733–741.

Drake, J.B., R.G. Knox, R.O. Dubayah, D.B. Clark, R. Condit, J.B. Blair, and M. Hofton, 2003. Above-ground biomass estimation in closed canopy neotropical forests using lidar remote sensing: Factors affecting the generality of relationships, *Global Ecology and Biogeography*, 12(2):147–159.

Efron, B., and R. Tibshirani, 1993. *An Introduction to the Bootstrap*, CRC Press. 456 p.

Gregoire, T.G., G. Stahl, E. Naesset, T. Gobakken, R. Nelson, and S. Holm, 2011. Model-assisted estimation of biomass in a LiDAR sample survey in Hedmark County, Norway, *Canadian Journal of Forest Research*, 41(1):83–95.

Hall, S.A., I.C. Burke, D.O. Box, M.R. Kaufmann, and J.M. Stoker, 2005. Estimating stand structure using discrete-return lidar: An example from low density, fire prone ponderosa pine forests, *Forest Ecology and Management*, 208(1-3):189–209.

Hudak, A.T., N.L. Crookston, J.S. Evans, M.J. Falkowski, A.M.S. Smith, P.E. Gessler, and P. Morgan, 2006. Regression modeling and mapping of coniferous forest basal area and tree density from discrete-return lidar and multispectral satellite data, *Canadian Journal of Remote Sensing*, 32(2):126–138.

Hudak, A.T., M.A. Lefsky, W.B. Cohen, and M. Berterretche, 2002. Integration of lidar and Landsat ETM+ data for estimating and mapping forest canopy height, *Remote Sensing of Environment*, 82(2-3):397–416.

Hyyppa, J., O. Kelle, M. Lehikoinen, and M. Inkinen, 2001. A segmentation-based method to retrieve stem volume estimates from 3-D tree height models produced by laser scanners, *IEEE Transactions on Geoscience and Remote Sensing*, 39(5):969 –975.

Jensen, J.L.., K.S. Humes, T. Conner, C.J. Williams, and J. DeGroot, 2006. Estimation of biophysical characteristics for highly variable mixed-conifer stands using small-footprint lidar, *Canadian Journal of Forest Research*, 36(5):1129–1138.

Kennedy, R.E., W.B. Cohen, and T.A. Schroeder, 2007. Trajectory-based change detection for automated characterization of forest disturbance dynamics, *Remote Sensing of Environment*, 110(3):370–386.

Kennedy, R.E., Z. Yang, and W.B. Cohen, 2010. Detecting trends in forest disturbance and recovery using yearly Landsat time series: 1. LandTrendr - Temporal segmentation algorithms, *Remote Sensing of Environment*, 114(12):2897–2910.

Kim, S., R.J. McGaughey, H.-E. Andersen, and G. Schreuder, 2009a. Tree species differentiation using intensity data derived from leaf-on and leaf-off airborne laser scanner data, *Remote Sensing of Environment*, 113(8):1575–1586.

Kim, Y., Z. Yang, W.B. Cohen, D. Pflugmacher, C.L. Lauver, and J.L. Vankat, 2009b. Distinguishing between live and dead standing tree biomass on the North Rim of Grand Canyon National Park, USA using small-footprint lidar data, *Remote Sensing of Environment*, 113(11):2499–2510.

Lim, K., P. Treitz, K. Baldwin, I. Morrison, and J. Green, 2003. Lidar remote sensing of biophysical properties of tolerant northern hardwood forests, *Canadian Journal of Remote Sensing*, 29(5):658–678.

Maltamo, M., J. Malinen, P. Packalén, A. Suvanto, and J. Kangas, 2006. Nonparametric estimation of stem volume using airborne laser scanning, aerial photography, and stand-register data, *Canadian Journal of Forest Research*, 36(2):426–436.

McGaughey, R.J., 2012. *FUSION/LDV: Software for LIDAR Data Analysis and Visualization*, Version 3.01, US Forest Service.

Means, J.E., S.A. Acker, B.J. Fitt, M. Renslow, L. Emerson, and C. Hendrix, 2000. Predicting forest stand characteristics with airborne scanning lidar, *Photogrammetric Engineering & Remote Sensing*, 66(11):1367–1371.

Meigs, G.W., R.E. Kennedy, and W.B. Cohen, 2011. A Landsat time series approach to characterize bark beetle and defoliator impacts on tree mortality and surface fuels in conifer forests, *Remote Sensing of Environment*, 115(12):3707–3718.

Næsset, E., 1997. Estimating timber volume of forest stands using airborne laser scanner data, *Remote Sensing of Environment*, 61(2):246–253.

Ørka, H.O., T. Gobakken, E. Næsset, L. Ene, and V. Lien, 2012. Simultaneously acquired airborne laser scanning and multispectral imagery for individual tree species identification, *Canadian Journal of Remote Sensing*, 38(02):125–138.

Packalén, P., and M. Maltamo, 2006. Predicting the plot volume by tree species using airborne laser scanning and aerial photographs, *Forest Science*, 52(6):611–622.

Packalén, P., and M. Maltamo, 2007. The k-MSN method for the prediction of species-specific stand attributes using airborne laser scanning and aerial photographs, *Remote Sensing of Environment*, 109(3):328–341.

Packalén, P., and M. Maltamo, 2008. Estimation of species-specific diameter distributions using airborne laser scanning and aerial photographs, *Canadian Journal of Forest Research*, 38(7):1750–1760.

Parker, R.C., and P.A. Glass, 2004. High-versus low-density LiDAR in a double-sample forest inventory, *Southern Journal of Applied Forestry*, 28(4):205–210.

Pascual, C., A. García-Abril, L.G. García-Montero, S. Martín-Fernández, and W.B. Cohen, 2008. Object-based semi-automatic approach for forest structure characterization using lidar data in heterogeneous *Pinus sylvestris* stands, *Forest Ecology and Management*, 255(11):3677–3685.

Pflugmacher, D., 2011. *Remote Sensing of Forest Biomass Dynamics Using Landsat-derived Disturbance and Recovery History and Lidar Data*, Oregon State University, Corvallis, Oregon. 182 p.

Popescu, S.C., R.H. Wynne, and J.A. Scrivani, 2004. Fusion of small-footprint lidar and multispectral data to estimate plot-level volume and biomass in deciduous and pine forests in Virginia, USA, *Forest Science*, 50(4):551–565.

Powell, S.L., W.B. Cohen, S.P. Healey, R.E. Kennedy, G.G. Moisen, K.B. Pierce, and J.L. Ohmann, 2010. Quantification of live aboveground forest biomass dynamics with Landsat time-series and field inventory data: A comparison of empirical modeling approaches, *Remote Sensing of Environment*, 114(5):1053–1068.

Ståhl, G., S. Holm, T.G. Gregoire, T. Gobakken, E. Næsset, and R. Nelson, 2011. Model-based inference for biomass estimation in a LiDAR sample survey in Hedmark County, Norway, *Canadian Journal of Forest Research*, 41(1):96–107.

Strunk, J., H. Temesgen, H.-E. Andersen, J.P. Flewelling, and L. Madsen, 2012a. Effects of lidar pulse density and sample size on a model-assisted approach to estimate forest inventory variables, *Canadian Journal of Remote Sensing*, 38(05):644–654.

Strunk, J.L., S.E. Reutebuch, H.-E. Andersen, P.J. Gould, and R.J. McGaughey, 2012b. Model-assisted forest yield estimation with light detection and ranging, *Western Journal of Applied Forestry*, 27(2):53–59.

Sullivan, A.A., R.J. McGaughey, H.-E. Andersen, and P. Schiess, 2009. Object-oriented classification of forest structure from light detection and ranging data for stand mapping, *Western Journal of Applied Forestry*, 24(4):198–204.

Tonolli, S., M. Dalponte, M. Neteler, M. Rodeghiero, L. Vescovo, and D. Gianelle, 2011. Fusion of airborne LiDAR and satellite multispectral data for the estimation of timber volume in the Southern Alps, *Remote Sensing of Environment*, 115(10):2486–2498.

Wulder, M.A., T. Han, J.C. White, T. Sweda, and H. Tsuzuki, 2007. Integrating profiling LIDAR with Landsat data for regional boreal forest canopy attribute estimation and change characterization, *Remote Sensing of Environment*, 110(1):123–137.

Zhang, C., and F. Qiu, 2012. Mapping individual tree species in an urban forest using airborne lidar data and hyperspectral imagery, *Photogrammetric Engineering & Remote Sensing*, 78(10):1079–1087.

(Received 1/23/13; accepted 8/21/13; final version 8/22/13)